LQG and Feedforward Controllers
for the Deep Space Network Antennas

W .K. Gawronski, C.S. Racho, and J.A. Mellstrom

Abstract. The controller development and the tracking performance evaluation for NASA's Deep Space Network antenna arc presented. A trajectory preprocessor, 1 QG (Linear Quadratic Gaussian) controller, feedforward controller, and their combination are designed, built, analyzed, and test ed. The antenna exhibits nonlinear behavior when the input to the antenna and/or the derivative of this input exceeds the imposed limits; for slewing and acquisition commands, these limits are typically violated. A trajectory preprocessor was designed to insure that the antenna behaves linearly, just to prevent nonlinear limit cycling, The est imator model for the 1 QG cent roller was ident ified from the data obtained from the field test. Based on an LQG balanced representation, a reduced order LQG cont roller was obtained. The feedforward controller and the combination of the LQG and feedforward controller were also investigated. The performance of the controllers was evaluated with the tracking errors (due to following a trajectory) and the disturbance errors (due to the disturbances acting on antenna). The LQG controller has good disturbance rejection properties, and satisfactory tracking errors. The feedforward controller has small tracking error, but poor disturbance rejection properties. The combined LQG a n d feedforward controller exhibits small tracking errors, as well as good disturbance rejection properties. However the cost of this performance is found in the complexity of the controller,

The authors are with the Jet Propulsion I aboratory, California Institute of Technology, Pasadena, CA **91109**

1

I. INTRODUCTION

THE NASA Deep Space Network (DSN) antennas, operated by the Jet Propulsion Laboratory, consist of several antenna types and are located at Goldstone (California), Canberra (Australia), and Madrid (Spain). The DSN serves as a communication tool for spat.c exploration. The DSS-13 antenna, a new-generation 34-m beam-waveguide antenna, is shown in Fig. 1. Future NASA missions will include low-Earth-orbiting satellites, which require significant] y higher tracking rates (up to 0.4 clcg/see), when compared to the deep space missions (0.004-0.01 clcg/see). Thus the servos for the antennas require upgrading in order to follow commands with the required precision. Some upgrade options are presented in this paper, and are illustrated with simulation results and with field measurements.

The existing PI controllers, depicted in Fig.2, satisfy the requirements for deep-space X-band (8.4-GHz) tracking, For a higher tracking rate, a si mple and reliable choice is the addition of a feedforward controller, described in Refs. [5], [6]. The model-based, Linear Quadratic Gaussian (LQG) controllers are an alternative to feedforward controllers. The LQG design approach for the DSN antennas is presented in Refs. [2], [3], [4], and [6]. This paper addresses the design and the implementation issues of the feedforward and LQG controllers and compares their performance.

The controllers under consideration were designed for a linear plant. However, the antennas can exhibit non-linear behavior (limit cycling) due to limits i mposed on the antenna input. In order to ensure proper performance, a trajectory preprocessor is introduced.

II. TRAJECTORY PREPROCESSOR

in the case of unpredicted commands or severe environmental conditions, the drives could be overloaded and damaged, In order to prevent this from happening, limits arc placed on the input rates and accelerations of DSN

antennas. Because of these imposed limits, the antenna dynamics becomes non-linear (for the antenna commands exceeding these limits). The antenna tracking commands are usually within these limits. However the limits are often challenged by antenna slewing commands and by wind disturbances. When slewing commands exceed these limits, this usually results in antenna limit cycling. To avoid limit cycles, a slewing controller, which is different from the tracking controller, was implemented. In order to use the same controller for both tracking and slewing modes, the commands for the slewing mode must be modified so that they do not violate the rate and acceleration limits, yet still move the antenna at the highest rate possible. This command modification can be performed with a trajectory preprocessor located in the control system (see Fig.3). The preprocessor limits the rate and acceleration of the command as described below,

The basic structure of the trajectory preprocessor is derived from the feedforward controller of a DSN antenna [5], [6]. This controller has been proven to have good tracking performance. For the preprocessor purposes, the controller is simplified by removing its integral part, and by replacing the linear part of the antenna model with the integrator. The nonlinear part (i.e., the rate and acceleration limiters) remains untouched.

A block diagram of the trajectory preprocessor is shown in Fig.4a, where SAT denotes saturation, and RL denotes rate limiter. Consider a trajectory $r(t)$, and let v_{max} and a_{max} be the maximum rate and acceleration which are allowed for an antenna command. 1 n this figure r_f is the preprocessed trajectory, $e = r-r_f$ is the preprocessor error, k is its gain, u is the rate command, u_L is the limited rate command, and u_f is the limited acceleration and rate command. The first step in verifying the preprocessor is to check its performance for the lifted limits on rate and acceleration, i.e., for the linear case (see Fig.4b). Hence one obtains:

$$u =; \ +kr-kr_f, \ \dot{r}_f = u \tag{la}$$

and from the above one obtains $\dot{r}_f + kr_f = \dot{r} + kr,$

3

$$r_f =: r \qquad \text{(1b)}$$

if the initial conditions for r and r_f are the same, It shows that if the command does not violate the rate and acceleration limits, and if the initial conditions are the same, the preprocessed trajectory is identical to the original one.

In the nonlinear regime, the equations for the discrete-time preprocessor are as follows:

a) input, $u(i)$:

$$u(i) = k(r(i) - r_f(i) + v(i)), \qquad \text{(2a)}$$

where $v(i)$ is the command rate the ith instant,
b) input saturation:

$$u_L(i) = \begin{cases} v_{max} & \textit{for } u(i) > v_{max} \\ -v_{max} & \textit{for } u(i) < -v_{max} \\ u(i) & \textit{otherwise} \end{cases} \qquad \text{(2b)}$$

c) input' rate limiter:

$$u_f(i) = \begin{cases} u_f(i\text{-}1) + Ta_{max} & \textit{for } u_L(i) > u_f(i\text{-}1) + Ta_{max} \\ u_f(i\text{-}1) - Ta_{max} & \textit{for } u_L(i) < u_f(i\text{-}1) - Ta_{max} \\ u_L(i) & \textit{otherwise} \end{cases} \qquad \text{(2c)}$$

d) integration of u_f:

$$r_f(i) = r_f(i\text{-}1) + Tu_f(i), \qquad (v_f(i) = u_f(i)) \qquad \text{(2d)}$$

where $v_f(i)$ is the rate of the preprocessed trajectory at the ith instant. In the case of violated limits, it is difficult to analytically evaluate the

performance of the preprocessor, but it can be done by simulating commands typical for the DSN antennas. Typical commands arc: step command (slewing an antenna), rate offset, trajectory acquisition, and medium rate azimuth trajectory (up to 0.4 dcg/see),

First, the preprocessing of the step command is illustrated. A step command as in Fig.5a, solid line, is preprocessed for the maximum rate $v_{max} = 0.4$ deg/see, and the maximum acceleration $a_{max} = 0,6$ deg/sec^2 which is "acceptable" to a controller, The preprocessed trajectory is shown in Fig. 5a, dashed line. Its rate does not exceed v_{max} (see Fig.5b, dashed line), and its acceleration does not exceed a_{max} *(see Fig.5c, dashed line),*

For the rate offset test a command with the constant rate of 0.3 deg/sec is preprocessed for the initial position of the preprocessed trajectory identical to the initial position of the original trajectory $(r_f(o) = r(0))$, and the zero initial rate of the preprocessed trajectory $v_f(0) = O$, while the initial rate of the original trajectory is nonzero, i.e., $v(o) = 0.3$ deg/sec (Fig.6). The original and preprocessed trajectories shown in solid and dashed lines, respective] y, demonstrate that the original trajectory is quickly approached by the preprocessed one, For the case where both initial conditions (position and rate) of the preprocessed trajectory are different than those of the original trajectory $(r_f(0) = 1$ deg, $v_f(0) = O$ deg/see, and $r(0) = O$ deg, $v(0) = 0.3$ deg/see), the preprocessed trajectory is shown in Fig.6, dash-dotted line. The original trajectory is acquired with the maximum speed and acceleration, and the difference between them approaches zero.

Finally, a trajectory as shown in Fig.7a with maximum rate 0.3 deg/sec is preprocessed for $v_{max} = 0,4$ deg/see, $a_{max} = 0.6$ deg/sec^2, where the initial conditions $(r_f(0) = 22$ deg, $v_f(0) = O$ deg/see) differ from the original trajectory $(r(0) = 24$ deg, $v(O) = 100$ dcg/see). The preprocessed trajectory is shown in the same figure with clashed line. After acquisition the maximal difference between the original and the preprocessed traj ectories is less than 0.1 mdeg, see Fig.7b, which is much smaller than the noise level in the antenna position error.

111. LQG CONTROLLER

An LQG controller for the antennas, see Fig. 8, consists of an estimator, PI gains, flexible mode gains, and the trajectory preprocessor. The identification of an estimator gain determination, and the reduction of the controller, are described below,

A. *Identification of the Estimator Model*

The antenna model used for the design of the estimator has two inputs (azimuth and elevation rates) and two outputs (azimuth and elevation positions), see Ref. [4], [6], However, the cross-coupling between azimuth input and elevation output, and elevation input and azimuth output, is much weaker than the coupling between azimuth input and azimuth output, and elevation input and elevation output (compare Figs.9 and 10). This fact allows one to ignore the cross couplings and to use two separate antenna models (for azimuth and elevation). This approach simplifies the design and implementation of the LQG controller. The following test was simulated to justify this approach. An LQG controller A was designed for the plant without cross-couplings, and an LQG controller B was designed for the plant with cross-couplings. The resulting controllers A and B were applied to the plant. The performances of both controllers were nearly identical.

The analytical models for the DSS-13 antenna such as those in Ref. [6] cannot be implemented as an estimator due to their uncertainties (such as finite element model structural mass, friction, or gearbox stiffness), In order to design a model-based controller, an antenna model must precisely mimic the antenna dynamics. For this reason, an antenna model was identified using field measurements, see Ref. [12], The field measurements were taken as follows. While the antenna was moving with a constant rate u_o, a random signal u was injected. Then the input $u_m = u_o + u$ and the output $y_m = y_o + y$ were measured, where y. and y were responses to u_o and u, respectivel y. The

6

signals u and y were determined by dctrending u_m and y_m. Next, the time series data were passed through a Harming filter to prevent spectral leakage during a Fast Fourier Transformation, see Ref. [1],

The magnitude of the transfer function, $|T(f)|$, and the coherence, $\gamma(f)$, were estimated using the filtered and detrended input u and output y vectors of *8192* samples each

$$|T(f)| = \frac{P_{uy}(f)}{P_{uu}(f)}, \qquad \gamma(f) = \frac{|P_{uy}(f)|^2}{P_{uu}(f)\, P_{yy}(f)} \qquad (3)$$

where f is frequency in Hz, $P_{uu}(f)$ is the power spectral density estimate of $u(t)$, $P_{yy}(f)$ *is* the power spectral density estimate of y(t), and $P_{uy}(f)$ is the cross-spectral density estimate of $u(t)$ and $y(t)$. The magnitude of the transfer function and the coherence are plotted versus frequency in Figs.9a,c.

The identified azimuth and elevation models were obtained in the state-space form triple (A_i, B_i, C_i), $i = az$, or el. In a future analysis only the azimuth model is presented in detail, and the subscript i is dropped to simplify notation' (details of the elevation model and cross-coupling models can be found in Ref. [12]). In this model the state vector x is of dimension n, the input u *is* of dimension p, the output y is of dimension q, and the matrices A, B, C are of dimensions $n \times n$, $n \times p$, and $q \times n$, respectively.

A model is identified using the identification software SOCIT (System/Observer/Controller Identification Toolbox), see Refs. [8], [9]. A state-space model, (A, B, C), *is* identified given the input-output data, sample period, and the number of observer Markov parameters. The order of the system was chosen to be 24, based on the system Hankel singular values. Next, the state-space representation was transformed into balanced coordinates, so that the matrix A was in a diagonally dominant form, with 2x2 diagonal blocks. The diagonal elements of the block represent the system darnping, while the off-diagonal elements represent natural frequencies at those modes.

7

The identified transfer function plot is presented in Fig.9b.

The antenna model includes an integrator (note that the input is the rate and the output is the position). Thus, some of the system poles are at zero. The SOCIT software, not developed for the systems with poles at zero, consistently identified a model with all non-zero poles. Nevertheless, some of the poles were located close to zero. This feature was corrected by shifting the close-to-zero poles to zero. Also, the identified model showed overdamped modes. This was readily corrected by reducing the modal damping in the balanced representation.

The signals were measured with a sampling frequency of 80 Hz. Since the transfer function of the identified model should reflect the antenna dynamics for frequencies below 10 Hz these signals were oversampled. The excess data in the oversampled signal was used to reduce noise intensity through averaging, In this way, a typical signal record of *8192* samples was reduced to 1638 samples.

B. Balanced LQG Controller

The design of the balanced LQG controller for the DSN antennas was described in detail in Refs. [4], [6]. The closed-loop system with an LQG controller is shown in Fig. 8, with the estimator state-space triple (' ,B,C), the estimated state of flexible part x_{ef}, the control input u, the output y, the estimated output y_e, the command r, the servo error e, the process noise v of intensity V, and the measurement noise w of intensity W. Both v and w are uncorrelated $V = E(vv^T), E(ww^T) = I, E(vw^T) = O$, E(v)= O, E(w) = O, where $E(.)$ is the expectation operator. The triple (A,B,C) is stabilizable and detectable. The identified plant model was augmented with the new state (integral of the error), thus its order is increased to $n = 25$. The task is to determine the controller gain (k_c) and esti mater gain (k_e) such that the performance index (J),

$$J = E \left[\int_0^\infty (x^T Q x + u^T u) dt \right] \tag{4}$$

is minimized, where Q is a positive semi-definite state weight matrix. The minimum for *J is* obta ed for the feedback $u = -k_c x$, where the gain matrix $k_c = B^T S_c$ is obtained from the solution S of the controller Riccati equation [10]

$$A^T S_c + S_c A - S_c B B^T S_c + Q = O \tag{5a}$$

The optimal estimator gain is given by $k_e = S_e C^T$, where *Se is* the solution of the estimator Riccati equation

$$A S_e + S_e A^T - S_e C^T C S_e + V = O. \tag{5b}$$

Denote a diagonal positive definite matrix M $= diag(\mu_i), i = 1,\ldots,n, \mu_i > O$. A state-space representation is LQG balanced if

$$S_e = S_e = M \tag{6}$$

In this case $\mu_i, i = 1,\ldots,n$ are the LQG characteristic values of *(A,B,C)*, *see* Jonckheere and Silverman [7], and Opdenacker and Jonckheere [11] for weights Q$= C^T C, V = B B^T$, and Gawronski [3] for a general case of weights.

Let *(A,B,C)* be a state-space triple of the open-loop antenna in the Moore balanced representation. For a diagonal weight matrix $Q = diag(q_i I_2)$, $i = 1,\ldots,n,$ the solution SC of (5a) is as follows [3]

$$S_c \cong diag(s_{ci} I_2), \quad s_{ci} \cong (\beta_{ci} - 1)/2\gamma_i^2, \quad \beta_{ci}^2 = 1 + 2q_i \gamma_i^2 / \zeta_i \omega_i \tag{7a}$$

and for a diagonal $V = diag(v_i I_2), i = 1,\ldots,n,$ the solution S_e of (5b) is

$$S_e \cong diag(s_{ei} I_2), \quad s_{ei} \cong (\beta_{ei} - 1)/2\gamma_i^2, \quad \beta_{ei}^2 = 1 + 2v_i \gamma_i^2 / \zeta_i \omega_i \tag{7b}$$

It is shown in [3] that for flexible structures the Moore and the LQG balanced representations are approximately collinear, i.e., such that the transformation 7 from the first to the second requires only re-scaling of the components

$$T \cong diag(t_1 I_2, t_2 I_2, \ldots . t_n I_2), \, t_i = (s_{ci} s_{ei})^{1/4} \tag{8a}$$

and the approximate balanced solution is a geometric average of SC and S_e

$$M = \sqrt{S_c S_e} \cong diag(\mu_i I_2), \quad \mu_i = \sqrt{s_{ci} s_{ei}}, \quad i = 1,\ldots,n \tag{8b}$$

a result useful in the controller reduction.

C. Reduced-Order Controller

Although the size of the controller is equal to the size of the plant, it is crucial from an implementation point of view to obtain a controller of the smallest possible dimension that preserves the stability and performance of the full-order controller. In order to ensure the stability of the closed-loop system, the open-loop system (plant model) cannot be excessively reduced in advance. Therefore, controller reduction becomes a part of the controller design,

For a flexible structure, such as a DSN antenna, an LQG balanced approach [3] produces a stable reduced-order controller, for which the reduction index σ_i

$$\sigma_i = \gamma_i^2 \mu_i \tag{9}$$

ranks the importance of the controller states, It combines the open- and closed-loop characteristic values of a system,

The plots of the index σ_i for azimuth and elevation are shown in Fig.11. In the azimuth axis case, the index σ_i is small for $i \geq 10$ when compared to σ_i for $i \leq 9$. Thus the azimuth axis controller order is chosen to be 9.

The state-space representation (A, B, C) of the reduced azimuth axis estimator is given in the appendix, along with the controller gains $k_c = [k_p, k_i, k_f]$, and the estimator gains k_e.

IV. FEEDFORWARD CONTROLLER

The tracking accuracy of fast moving objects can be improved if a PI controller is augmented with a feedforward loop, see Refs. [5], [6]. A block diagram of the PI controller with the feedforward loop is shown in Fig. 12. In this block diagram, G, K, and F denote transfer functions of the antenna's rate loop, PI controller, and feedforward gain, respectively; r is a command, y is the output (elevation and azimuth angles), e is the tracking error in azimuth and elevation, and u is the plant input.

In the absence of disturbances, perfect tracking $(e=0)$ is obtained for the feedforward gain F such that $GF=1$. In the case of the Deep Space Network antennas, this condition is satisfied in a low frequency range of $0 \le f \le 1$ Hz for $F=s$, since for these frequencies the plant transfer function G can be approximated with an integrator $G=1/s$.

The DSS-13 antenna PI controller, with proportional gain $k_p=0.5$ and integral gain $k_i=0.5$ in azimuth and elevation, was investigated. The closed-loop transfer function (azimuth command to azimuth encoder) for a system with and without the feedforward gain is compared in Fig. 13. The figure shows that for frequencies up to 1 Hz the system with the feedforward gain has better tracking properties when compared to the system without feedforward gain (good tracking properties are characterized by the unit value of the magnitude of the transfer function),

V. LQG-AND-FEEDFORWARD CONTROLLER

The controller performance is usually tested for tracking errors when

following a command, and for servo errors due to wind disturbances. Therefore the tracking and disturbance rejection properties have to be traded off. The feedforward controller for the DSN antennas has good tracking properties, confirmed by both simulations and field measurements. Also, its performance during the slewing maneuver is satisfactory, since no limit cycling is observed. However the feed forward controller ability to compensate for wind action is insufficient, and its disturbance rejection properties are equivalent to those of a PI controller. On the other hand, the LQG controller is effective in suppressing wind induced vibrations, but has weaker tracking properties.

In comparing the properties of feedforward and LQG controllers, one can conclude that by combining the two it is possible to improve both the tracking and disturbance rejection properties. The properties of a combination of the LQG and feedforward controllers were derived for a system configured as shown in Fig. 14. In this block diagram, G is the plant transfer function, G_y is the estimator transfer function from y to y_e, G_{yu} is the estimator transfer function from u to y_e, G_{uy} is the estimator transfer function from y to u_e, and G_u is the estimator transfer function from u to u_e. In determining the feedforward transfer function F, note that good tracking properties are required for low frequencies only (in our case for frequencies up to 1 Hz). For these frequencies, $G_{yu} \cong 0$, and $G_y \cong 1$, thus $y_e \cong y$. For the system as in Fig. 14 (assume transfer function of the trajectory preprocessor equal to 1, i.e., $r = r_f$):

$$e = r - y_e, \quad y = Gu, \quad u = Fr + Ke + G_f G_u u + G_f G_{uy} y, y_e = G_{yu} u + G_y y. \tag{lo}$$

From these equations one obtains

$$e = \frac{H - G_{yu} F - G_y GF}{H + G_y GK + G_{yu} K} r, \quad H = 1 + G_f G_u + G_f G_{uy} G. \tag{11}$$

The servo error is eliminated (i.e., $e = 0$) if the numerator of the above transfer function is zero. This is true for the following feedforward

transfer function:

$$F = \frac{1 + G_f G_u \mathbf{i} - G_f G_{uy} G}{s G_{yu} + G_y} .$$

(12)

For the low frequencies $(f < 2 \ Hz)$ the following is true: $G = 1/s$, $G_f G_u$ is constant $(G_f G_u = k_u$, where k_u is the dc gain of $G_f G_u$), $G_{yu} \cong 0$, $G_y = 1$, and $G_f G_{uy} \cong k_{uy} s$. Thus F in Eq,(12) **represents a differentiator**

$$F = k_{ff} s, \qquad k_{ff} = 1 + k_u + k_{uy}$$

(13)

with the gain $k_{ff} = 1 + k_u + k_{uy}$, called the feed forward gain.

The result (13) was tested as follows, The LQG controller was configured as in the previous section; the dc gains were $k_u = 2.23$, $k_{uy} = -0.58$. The maximal tracking errors of this LQG controller with a feedforward gain were observed . in the simulations for different values of the gain k_{ff}, and are shown in Fig. 15. The minimum tracking error is achieved for the feed forward gain $k_{ff} = 1 + k_u + k_{uy} = 2.65$.

VI, PERFORMANCE EVALUATION

The position error for a trajectory which approaches antenna rate and acceleration limits, and the position error due to disturbances, are used as performance measures of the antenna position controllers, The performance of the LQG and feed forward controllers for the DSS - 13 antenna (Fig. 1) was evaluated through simulations and tested in the field. For this antenna the rate limit is set to 0.36 deg/see, and the acceleration limit is set to 0.2 deg/sec². The acquisition and tracking of the trajectory shown in Fig.7a was measured. At time O sec the spacecraft is at position 24 deg, and the antenna is at position 22 deg. The trajectory preprocessor was activated in this case, and the preprocessed trajectory is shown in Fig.7a, dashed line,

13

For the PI controller (k_p =0.5, k_i = O. 5) the tracking error is shown in Fig.16a,b. Figure 16a shows the transient tracking error due to the initial step. Figure 16b is a zoom of the same tracking error plot in Fig. 16a which gives a higher resolution view of the magnitude of the tracking error. The maximal value of the error is 28 mdeg (see also Table 1), which is beyond the required accuracy of 5 mdeg.

The acquisition of the trajectory for the same PI controller with a feedforward gain and without a trajectory preprocessor is shown in Fig. 17a. After acquiring the target, the maximal tracking error is **2.5** mdeg (see Fig, 17 b). However, there are poorly damped oscillations present in these data plots.

The performance of the LQG controller with the PI gains $k_p = 12, k_i = 10$ was measured and is shown in Fig. 18. The maximal tracking error is 3.7 mdeg, as in the case of the feedforward controller, but the flexible deformations were much more effectively damped by the LQG controller,

The LQG controller with the PI parameters $k_p = 12, k_i = 10$ and a feed forward loop (for the feed forward gain $k_{ff} = 3$) was tested. The results are shown in Fig. 19. They show a very small tracking error of 1,5 mdeg, and flexible mode suppression that is similar to the LQG controller.

The accuracy of the antenna model was tested by comparing measured (solid line) and simulated (dashed line) data in Fig.20 for the case of the LQG controller with PI gains $k_p = 12$, $k_i = 10$. The figure shows good agreement between the two data (which would improve in the absence of encoder faults).

The disturbance rejection properties of the presented controllers were simulated. The use of simulations instead of field measurements is justified for two reasons, First, it is difficult, if not impossible, to repeat the same disturbance" conditions in the field so that fair comparisons could be made. Secondly, the accuracy of the antenna model has been proved experimentally. The disturbance white noise, w, with standard deviation 0.005

ctcg/see, was added to the input u. This noise intensity is approximately equivalent to a 30 mph wind acting on the antenna. The simulation results (rms error, mdeg) are shown in the second row of Table 1. The results show good disturbance rejection properties of the LQG and LQG-with-feedforward controllers, when compared with PI and PI-with-feedforward controllers. Note the good coincidence of simulated and measured results for the PI and the LQG controllers. For these controllers the signal-to-noise ratio was high. On the other hand, for the feed forward, and the LQG-with-feedforward controllers the signal-to-noise ratio was low. Hence this signal was engulfed in noise, and the evaluation of tracking error from the noisy measured data could only be approximated within the noise level.

Table 1. Tracking and disturbance errors (mdeg)

	PI	FF	LQG	LQG+FF
Tracking error (maximal)	28.6	0,7	3.6	0.1
Disturbance error (rms)	3,2	3.6	0.4	0.5
Measured error (maximal)	28.0	2.5	3.7	1.5

VII, CONCLUSIONS

The new controllers were' designed and tested to improve the DSN antenna tracking performance. The measures of such improvement are the reduction in position error for a trajectory which approaches antenna rate and acceleration limits, and the reduction in position error due to disturbances. The results of running the new control algorithms on the DSS - 13 antenna show an improvement in the performance of the LQG, feed forward, and LQG-with-' feedforward controllers over the existing PI controller. On the other hand, the feedforward controller achieves good performance while remaining simple (avoids the complexity of the estimator and pre-processor), but its ability to suppress disturbances is limited. The LQG controller alone shows greatly improved disturbance rejection properties. However, the most i reproved performance was observed for the combination of the LQG and feedforward controller, It had very small tracking and disturbance-induced errors.

15

The trajectory preprocessor was introduced as a necessary part of the implementation of the LQG controller, so that tracking and slewing could be accomplished with one algorithm. In current operation, the PI controller requires separate modes for tracking and slewing due to the limit cycling which occurs in the latter. However, the preprocessor can also be implemented with the existing PI controller to combine tracking and slewing into a single mode.

ACKNOWLEDGMENTS

REFERENCES

[1]   J.S. Bendat and A. G. Piersol, *Random Data: Analysis and Measurement Procedures,* 2nd Edition, Wiley, New York, 1986.

[2]   W. Gawronski, "Design of a Linear Quadratic Controller for the Deep Space Network Antennas, " *Journal of Guidance, Control, and Dynamics,* accepted for publication (also *Proc. 1992 AIAA Guidance, Navigation, and Control Conf.,* Hilton Head, SC, pp. 1399-1408, 1992).

[3]   W. Gawronski, "A Balanced LQG Compensator for Flexible Structures, " accepted for publication in *A utomatica* (also *Proc. 1993 IEEE American Control Conference,* San Francisco, 1993),

[4]   W. Gawronski, "Design of the Reduced LQG Compensator for the Deep Space Network Antennas, " *Proc.* 1993 *AIAA Guidance, Navigation, and Control Conf.,* Monterey, CA, pp. *243-253,* 1993.

[5]   W. Gawronski and J.A. Mellstrom, "Antenna Servo Design for 'Tracking Low-Earth-Orbit Satellites," accepted for publication in *Journal of Guidance, Control, and Dynamics* (also *Proc.* 1994 *AIAA Guidance, Navigation, and Control Conf.,* Scottsdale, AZ, August 1-3, 1994),

[6]   W, Gawronski and J.A. Mellstrom, "Control and Dynamics of the Deep Space Network Antennas," a chapter in *Control and Dynamic System,* vol. 67, ed. C.T. Leondes, Academic Press, San Diego, CA, 1994.

[7]   E.A. Jonckheere and L.M. Silverman, "A New Set of Invariant for Linear Systems - Application to Reduced Order Compensator Design," *IEEE Trans. Automat. Control,* vol. AC-28, no,' 10, 1983,

[8]   J.-N. Juang, *Applied System Identification,* Prentice Hall, Englewood Cliffs, NJ, 1994.

[9]   J.-N. Juang, M. Phan, L, G. Horta and R.W. Longman, "Identification of Observer and Kalman Filter Markov Parameters: Theory and Experiment," *Proc. of the AIAA Guidance, Navigation, and Control Conf., New* Orleans, LA, 1991, pp. 1172-1179.

[10] H, Kwakernaak and R. Sivan, *Linear Optimal Control Systems,* Wiley-Interscience, New York, 1972.

[11] P. Opdenacker and E.A. Jonckheere, "LQG Balancing and Reduced LQG Compensation of Symmetric Passive Systems," *Int. J. Control,* VO1.41, no.1, pp.73-109, 1985,

[12] C.S. Racho and W. Gawronski, "Experimental Modification and Identification of the DSS- 13 Antenna Control System," *TDA Progress Report, 42-115,* July-September 1993, Jet Propulsion Laboratory, California Institute of Technology (1993), pp.42-53.

Estimator triple (A, B, C), where $C^{\mathrm{T}} = [C_{\mathrm{p}}^{\mathrm{T}} \; C_{\mathrm{f}}^{\mathrm{T}}]$, and gains $k_{\mathrm{p}}, k_{\mathrm{i}}, k_{\mathrm{f}}, k_{\mathrm{e}}$

$$
A = \begin{vmatrix}
1 & -0.01955 & 0.18642 & -0{,}03930 & 0.12127 & 0{,}01232 & 0.08334 & -0.07823 & -0.09326 \\
0 & 0.95945 & -0.20718 & -0.00937 & -0.00554 & -0{,}00758 & -0.00154 & -0.00485 & 0.00974 \\
0 & 0{,}20718 & 0.97580 & -0{,}00508 & -0.00194 & -0.00415 & -0.00051 & -0.00222 & 0.00489 \\
0 & -0.00937 & 0.00508 & 0.85543 & -0.49999 & -0.00046 & -0.01739 & -0.00905 & 0.01219 \\
0 & 0000554 & -0.00194 & 0.49999 & 0.85764 & -0.04976 & 0.00209 & -0.01013 & 0.02416 \\
0 & -0.00758 & 0{,}00415 & -0.00046 & 0.04976 & 0.91026 & -0.38398 & -0.01464 & 0.02037 \\
0 & 0.00154 & -0.00051 & 0.01739 & 0.00209 & 0.38398 & 0.92094 & -0.00771 & 0.01805 \\
0 & 0.00485 & -0.00222 & ``0.00905 & -0.01013 & 0.01464 & -0000771 & 0.93139 & 0.33443 \\
0 & 0.00974 & -0.00489 & 0.01219 & -0.02416 & 0{,}02037 & -0.01805 & -0.33443 & 0.83555
\end{vmatrix}
$$

$B^{\mathrm{T}} = 0.01 \times [0.231 \;\; 1.785 \; -0.395 \;\; 0.485 \; -0.211 \;\; 0.395 \; -0.055 \; -0.230 \;\; -0.479]$

$\mathrm{Cp} = [1\,o\,o\,o\,o\,o\,o\,o \quad o]$,

$C_{\mathrm{f}} = [0_{8 \times 1} \;\; I_8]$

$k_{\mathrm{p}} = 12$,

$k_{\mathrm{i}} = 10$,

$k_{\mathrm{f}} = [17.163 \;\; 13.586 \;\; 6.300 \;\; 1.829 \;\; 4.929 \;\; 1.869 \;\; 0.231 \;\; -3.299]$

$k_{\mathrm{e}}^{\mathrm{T}} = [0.9955 \;\; -0.1098 \;\; 0.2217 \; -0.1710 \;\; 0.2090 \; -0.1000 \;\; 0.1682 \;\; 0.0131 \;\; -0.0785]$
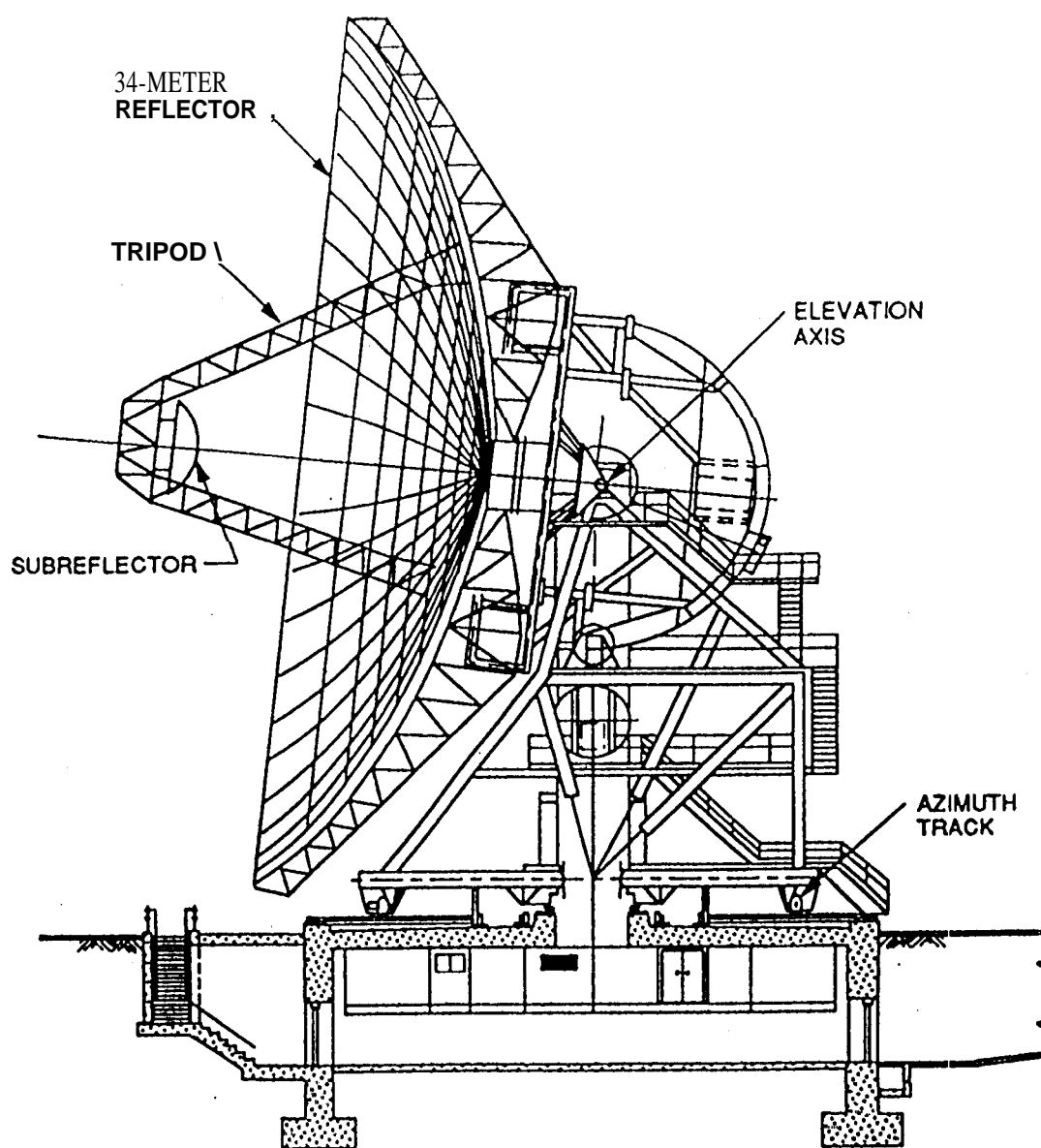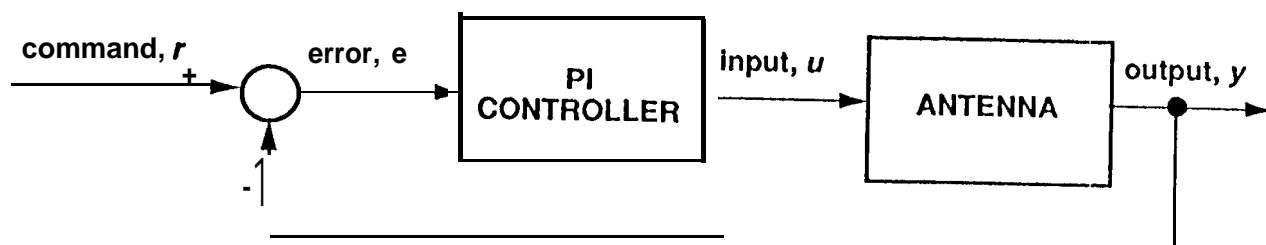
34-METER **REFLECTOR**

TRIPOD \

SUBREFLECTOR

ELEVATION AXIS

AZIMUTH TRACK

Gawronski, Racho, and Mellstrom

command, _r_
+
error, e
PI CONTROLLER
input, _u_
ANTENNA
output, _y_
-1

Gawronski, Racho, and Mellstrom
Fig.2

command, _r_
TRAJECTORY PREPROCESSOR
r_f
+
error, _e_
PI CONTROLLER
input, _u_
ANTENNA
output, _y_
~

Gawronski, Racho, and Mellstrom
Fig.3

a)

SIMPLIFIED ANTENNA MODEL

b)
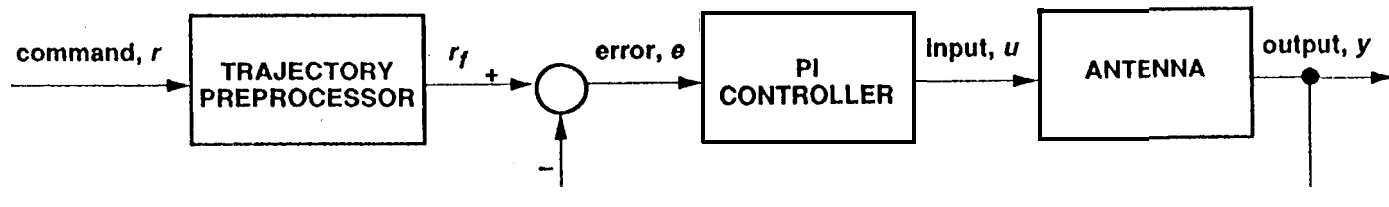
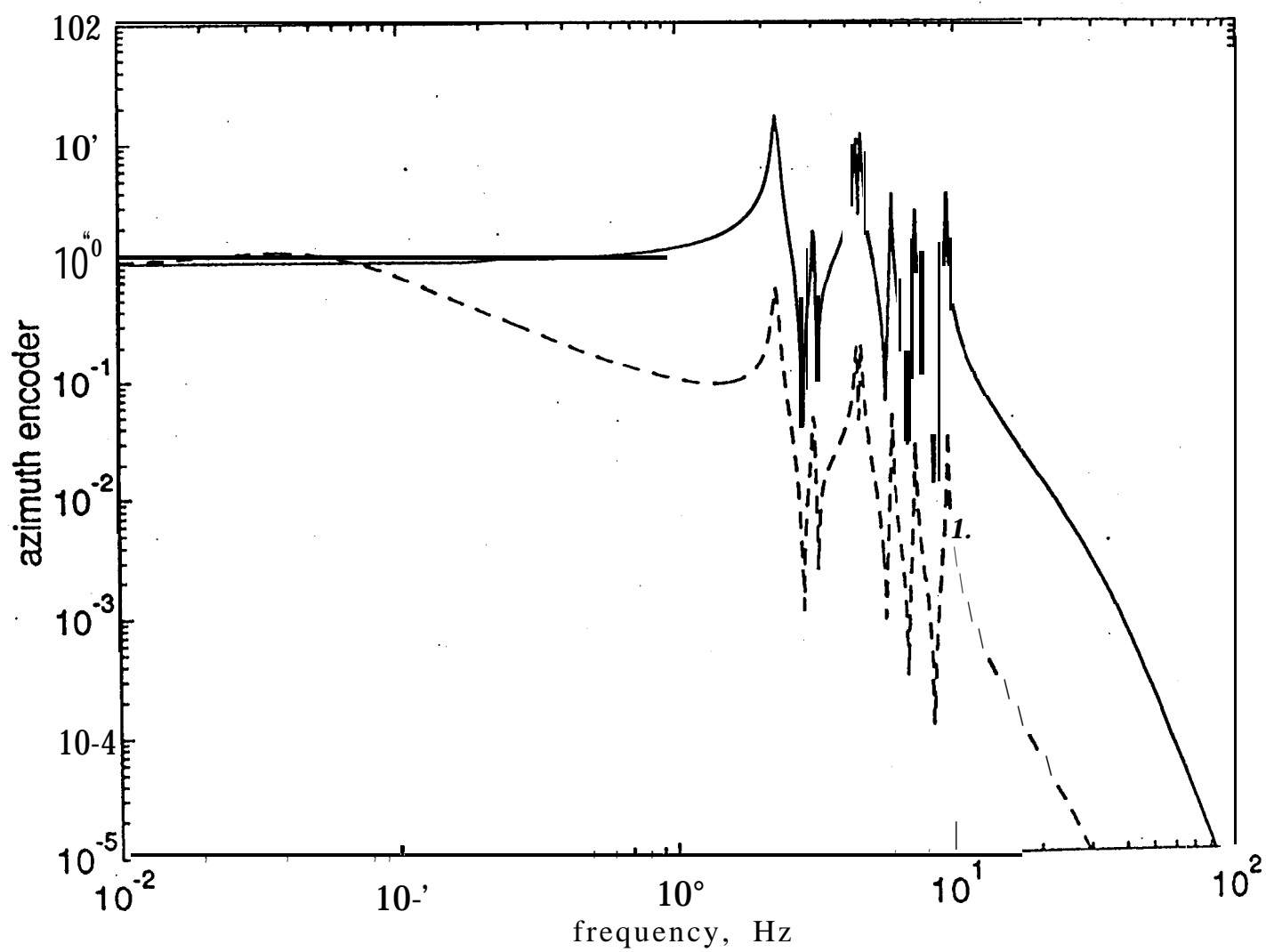Gawronski, Racho, and Mellstrom
Fig.4
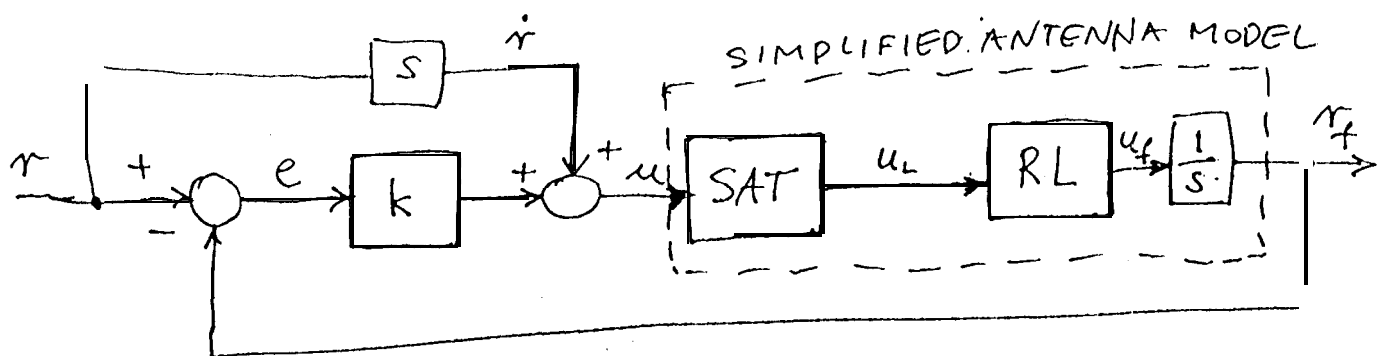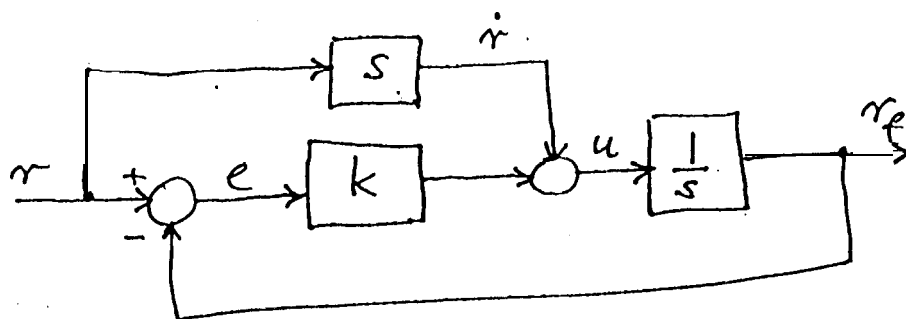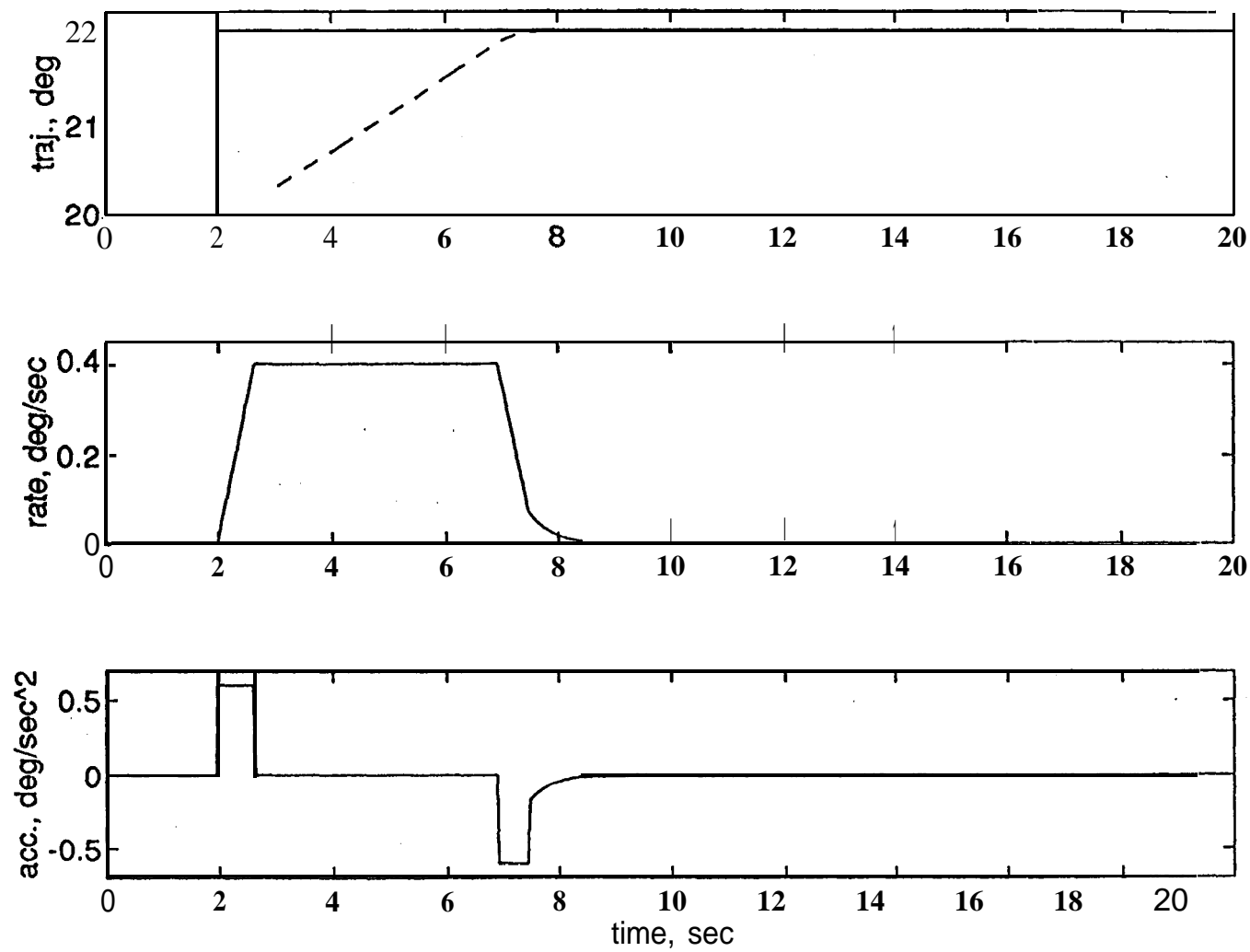
Gawronski, Racho, and Mellstrom
Fig.5

Gawronski, Racho, and Mellstrom
Fig. 8
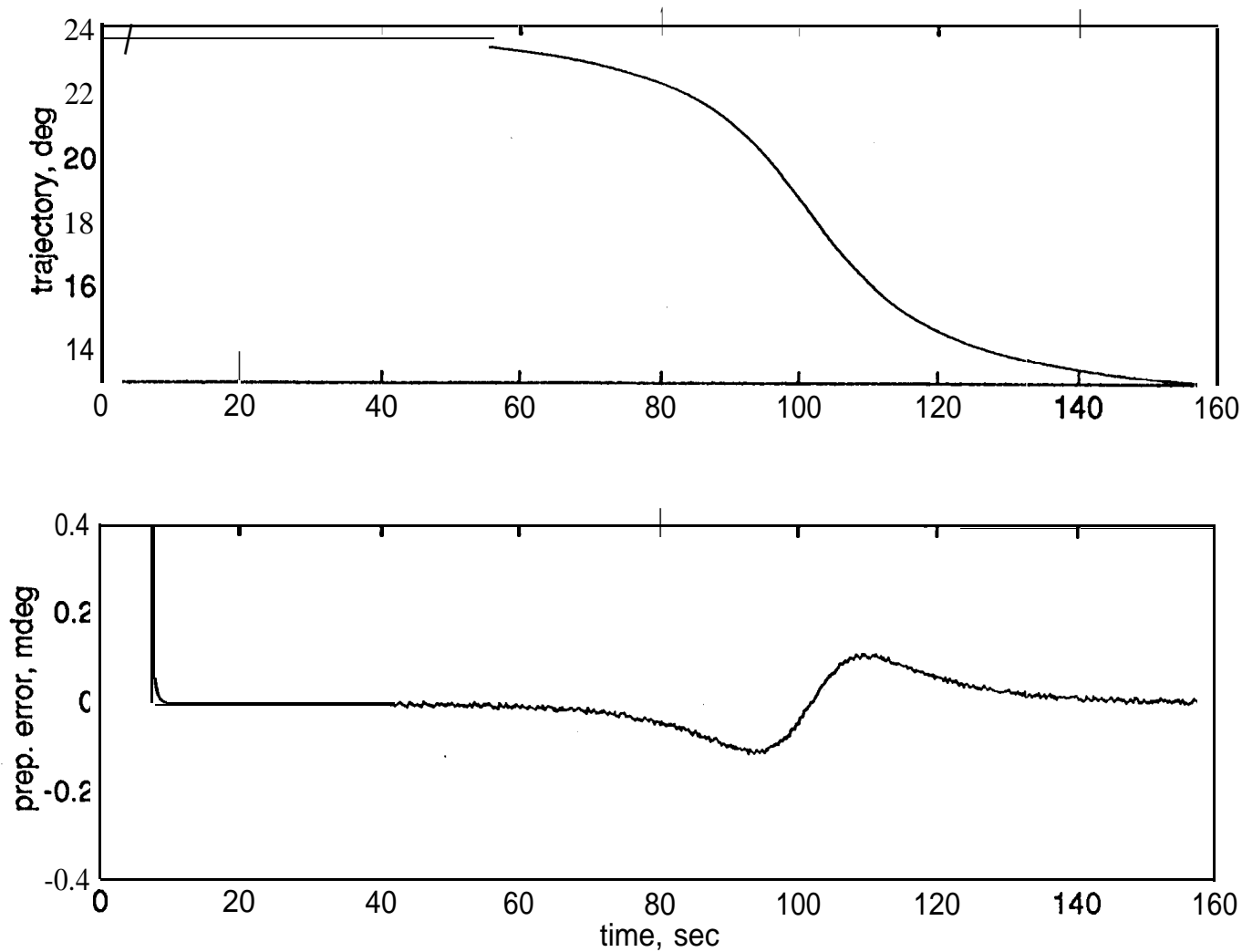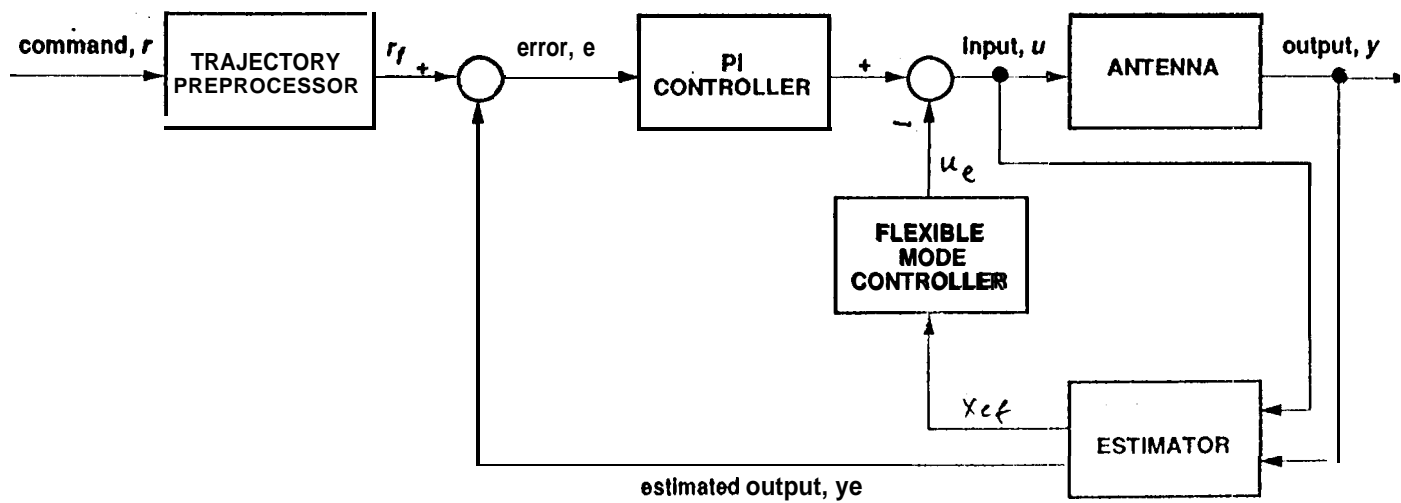
MAGNITUDE

MAGNITUDE

COHERENCE

FREQUENCY, Hz

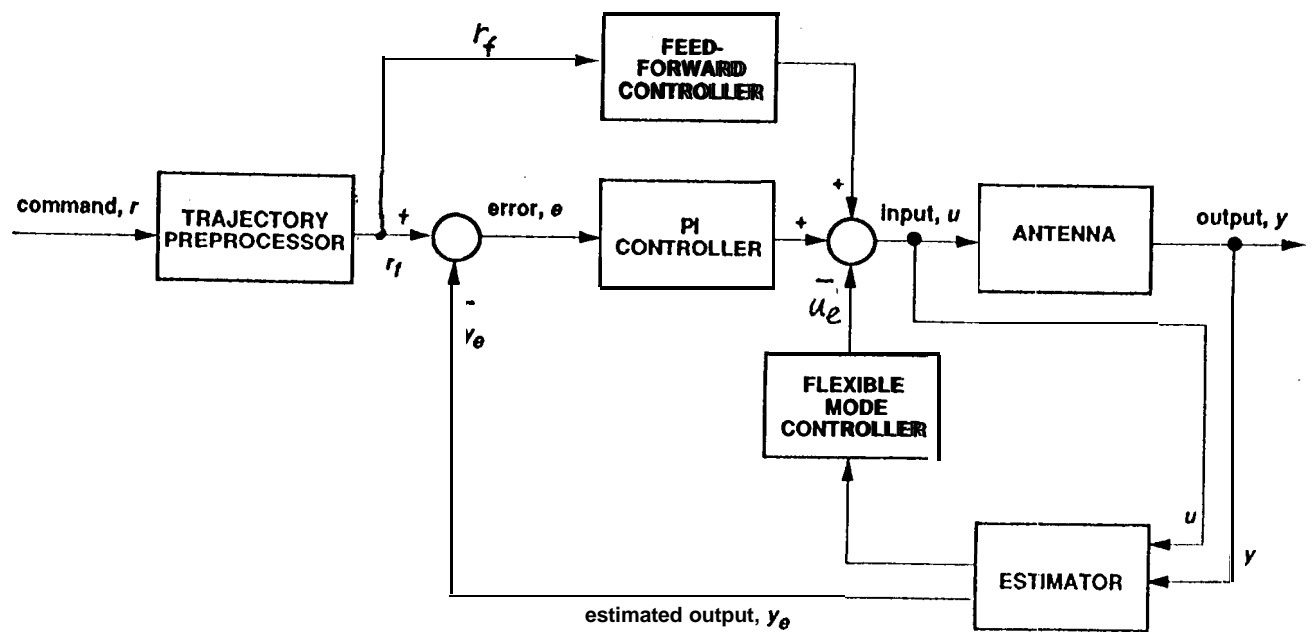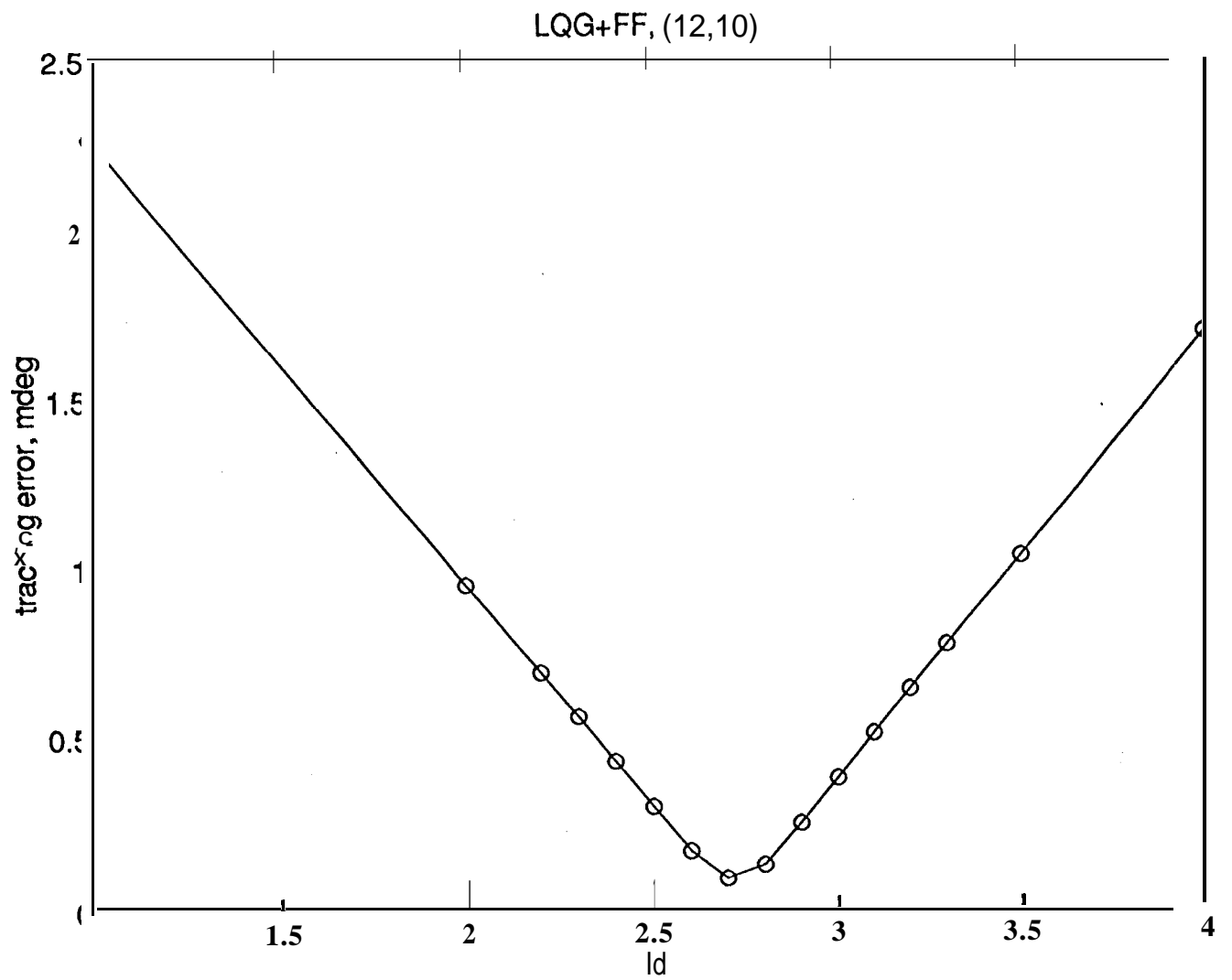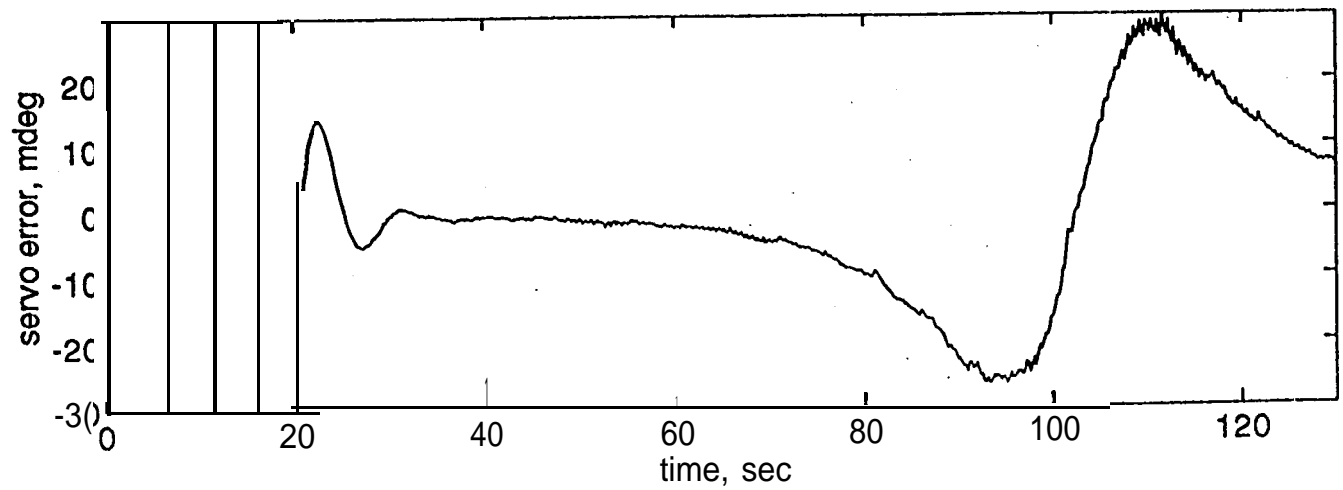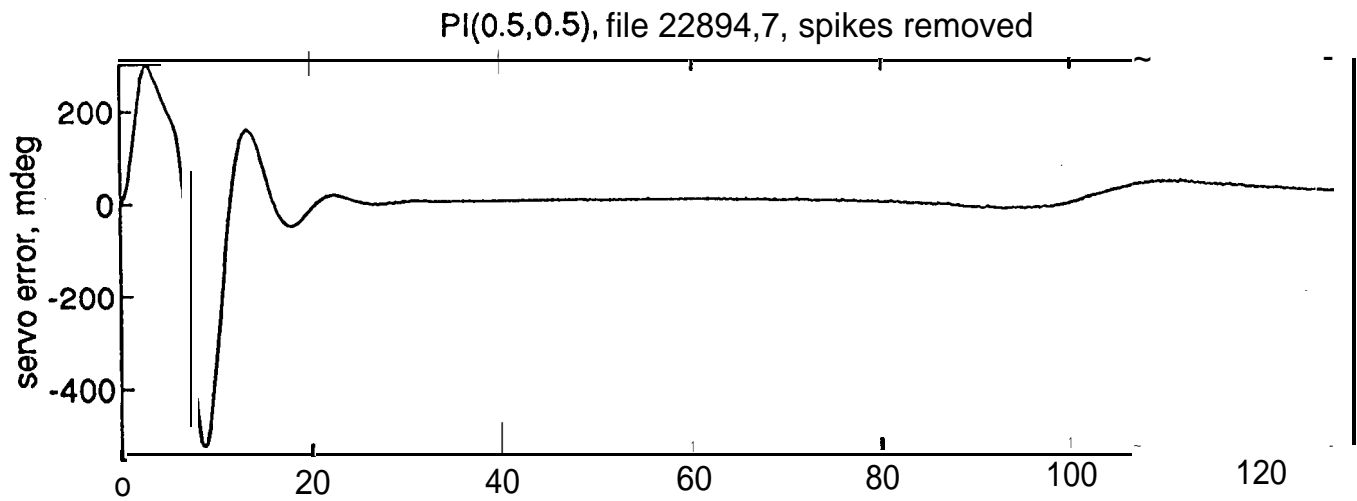Gawronski, Racho, and Mellstrom
Fig. 9

(a)

MAGNITUDE

FREQUENCY, Hz
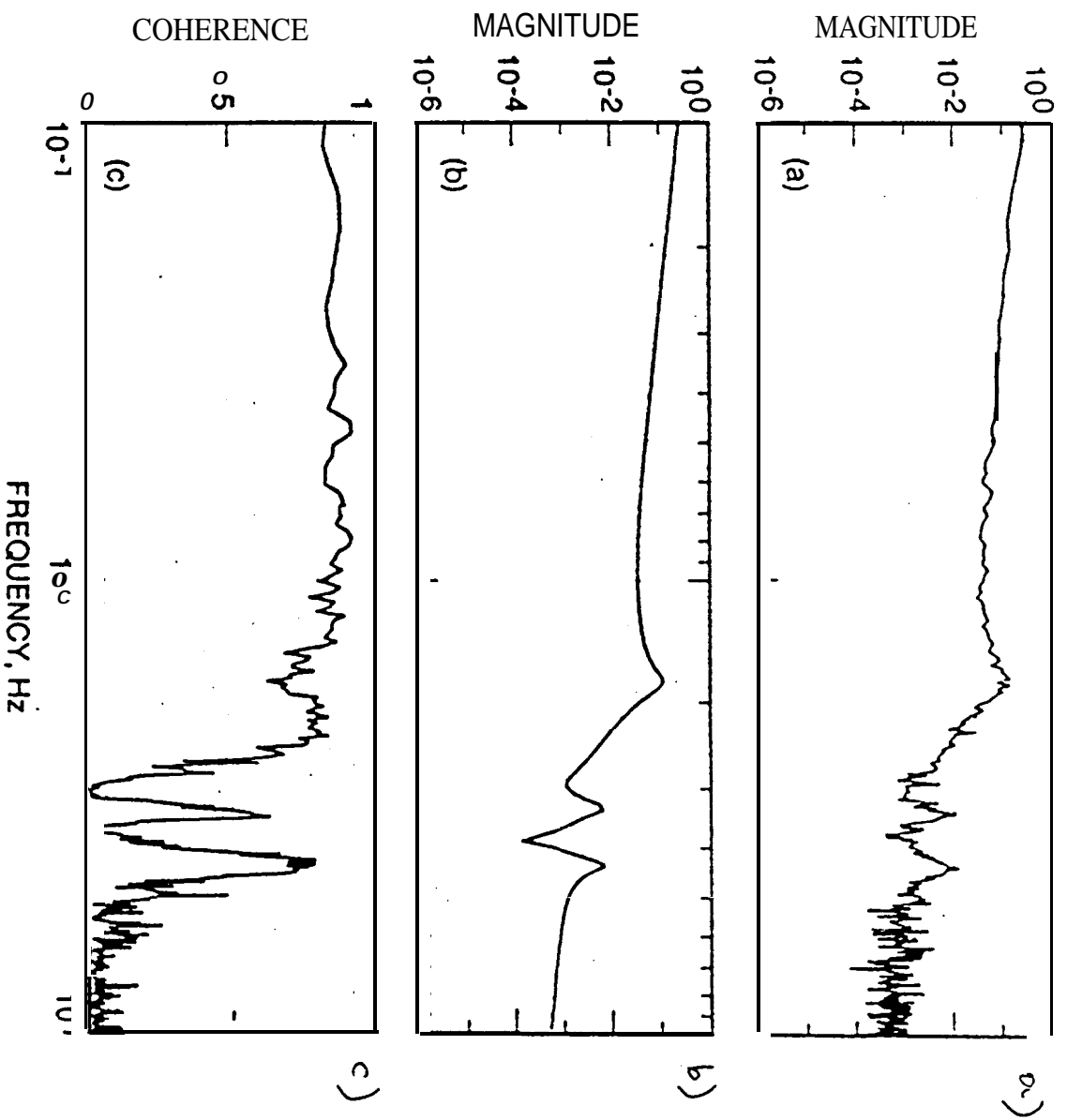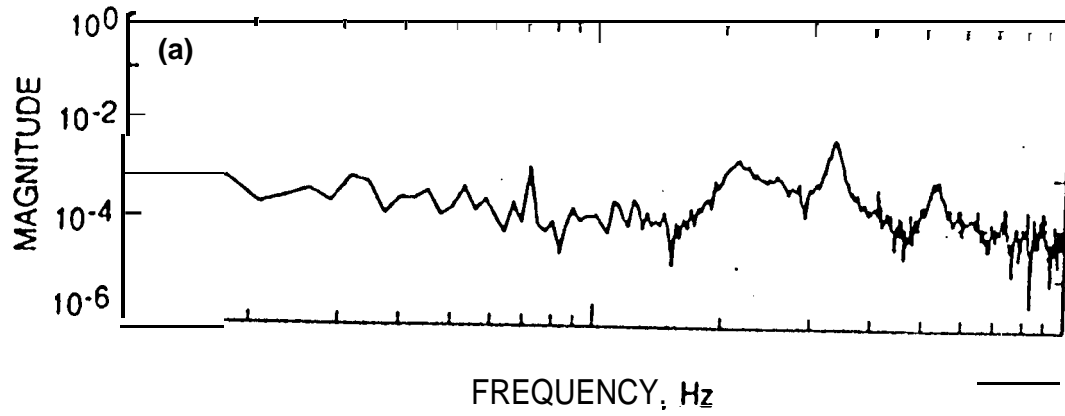
Gawronski, Racho, and Mellstrom
Fig.10

Gawronski, Racho, and Mellstrom
Fig.11

FEED-
FORWARD
CONTROLLER
F

command, r → TRAJECTORY PREPROCESSOR → v_f / r_f + → error, e → PI CONTROLLER K → + → input, u → ANTENNA G → Output, y

$-$ Y

Gawronski, Racho, and Mellstrom
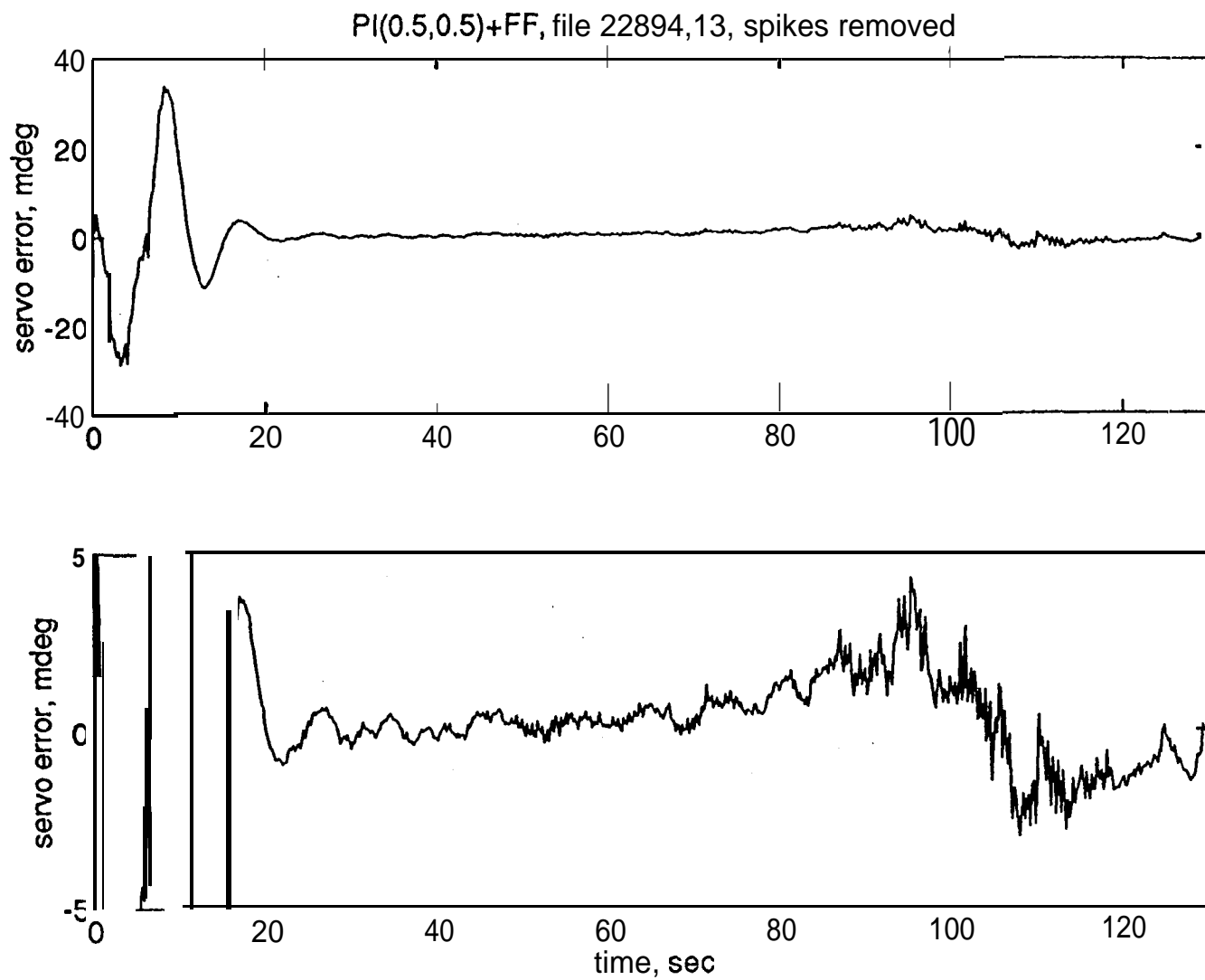Fig.12

Gawronski, Racho, and Mellstrom
Fig.13

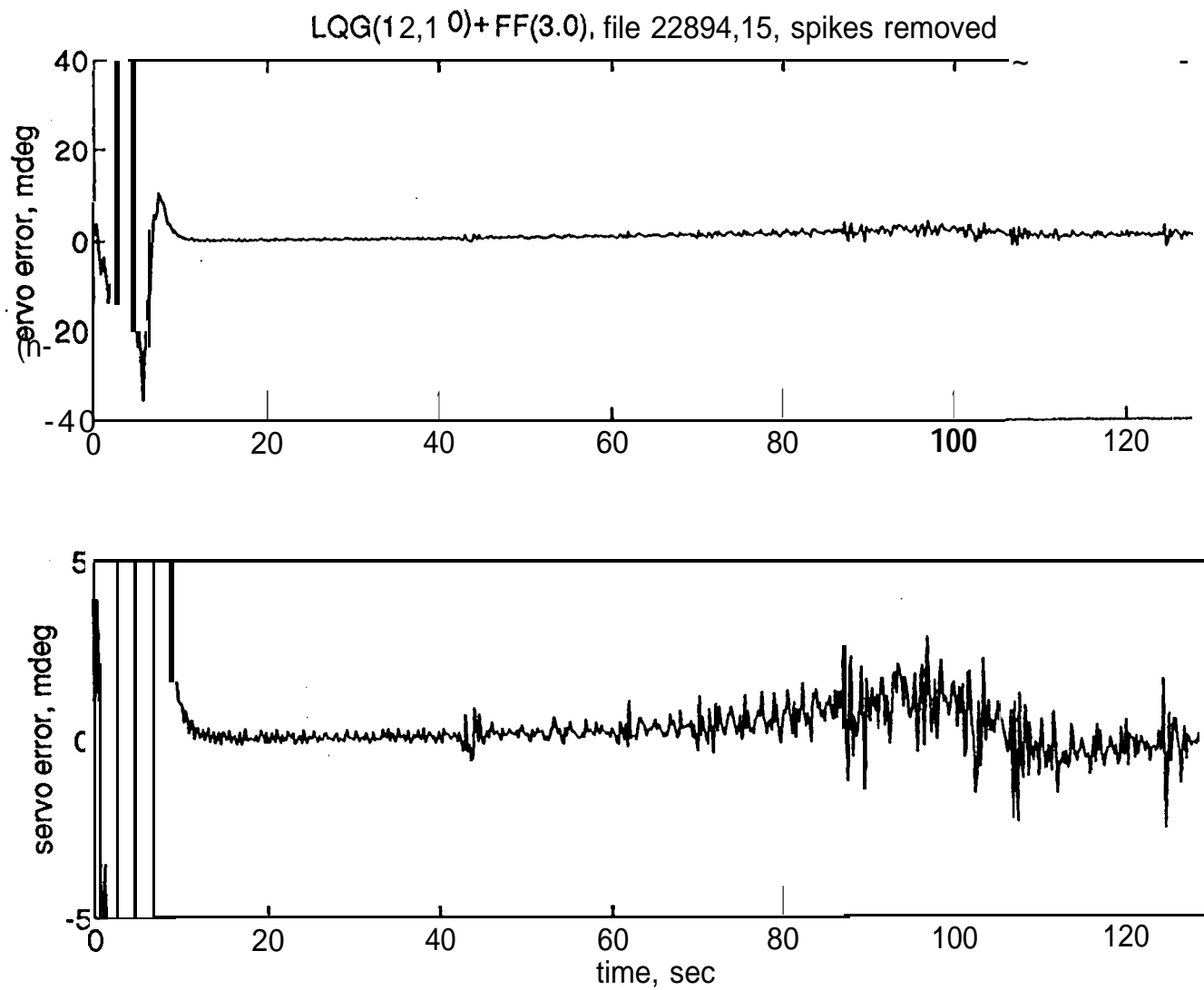command, r → TRAJECTORY PREPROCESSOR

r_f

FEED-FORWARD CONTROLLER

error, e → PI CONTROLLER

Input, u → ANTENNA → output, y

FLEXIBLE MODE CONTROLLER

ESTIMATOR

estimated output, y_e

Gawronski, Racho, and Mellstrom
Fig. 14a,b

LQG+FF, (12,10)

Gawronski, Racho, and Mellstrom
Fig. 15--------

PI(0.5,0.5), file 22894,7, spikes removed

Gawronski, Racho, and Mellstrom
Fig.16a.b

PI(0.5,0.5)+FF, file 22894,13, spikes removed

Gawronski, Racho, and Mellstrom

LQG(12,1 O), file 22894,11, spikes removed

Gawronski, Racho, and Mellstrom
Fig.18a,b

LQG(12,1⁰)+FF(3.0), file 22894,15, spikes removed

Gawronski, Racho, and Mellstrom
Fig. 19a,b

LQG(1 2,10), file 228%11, _ measured, --- simulated, spikes removed

Gawronski, Racho, and Mellstrom
Fig.20a,b